The Journal of Undergraduate Research in Physics

CONTENTS

VOLUME 8, NUMBER 2

APRIL 1990

Published by the Physics Department of Guilford College
for
The American Institute of Physics and The Society of Physics Students

THE JOURNAL OF UNDERGRADUATE RESEARCH IN PHYSICS

This journal is devoted to research work done by undergraduate students in physics and its related fields. It is to be a vehicle for the exchange of ideas and information by undergraduate students. Information for students wishing to submit manuscripts for possible inclusion in the Journal follows.

ELIGIBILITY

The author must have performed all work reported in the paper as an undergraduate. The subject matter of the paper is open to any area of pure or applied physics or physics related field.

SPONSORSHIP

Each paper must be sponsored by a full-time faculty member of the department in which the research was done. A letter from the sponsor, certifying that the work was done by the author as an undergraduate and the the sponsor is willing to be acknowledged in the paper, must accompany the manuscript if it is to be considered for publication.

SUBMISSION

Two copies of the manuscript, the letter from the sponsor and a telephone number where the author can be reached should be sent to:

Dr. Rexford E. Adelberger, Editor
THE JOURNAL OF UNDERGRADUATE
RESEARCH IN PHYSICS
Physics Department
Guilford College
Greensboro, NC 27410

FORM

The manuscript should be typed, double spaced, on 8 1/2 x 11 inch sheets. Margins of about 1.5 inches should be left on the top, sides, and bottom of each page. Papers should be limited to fifteen pages of text in addition to an abstract (not to exceed 250 words) and appropriate drawings, pictures, and tables. Manuscripts may be submitted on a disk that can be read by a MacIntosh™. The files must be compatible with MacWrite™ or MicroSoft Word™. Illustrations should be in a MacDraw™ or MacPaint™ PICT format.

ILLUSTRATIONS

Line drawings should be made with black ink on plain white paper. Each figure or table must be on a separate sheet. Photographs must have a high gloss finish.

CAPTIONS

A brief caption should be provided for each illustration or table, but it should not be part of the figure. The captions should be listed together at the end of the manuscript

EQUATIONS

Equations should appear on separate lines, and may be written in black ink.

FOOTNOTES

Footnotes should be typed, double spaced and grouped together in sequence at the end of the manuscript.

SUBSCRIPTION INFORMATION

The Journal is published bianually, with issue one appearing in October and issue two in April of the next year. There are two issues per volume.

TYPE OF SUBSCRIBER	PRICE PER VOLUME
Individual	$US 5.00
Institution	$US 10.00

Foreign subscribers add $US 2.00 for surface postage, $US 10.00 for air freight.

To receive a subscription, send your name, address, and check made out to **The Journal of Undergraduate Research in Physics (JURP)** to the editorial office:

JURP
Physics Department
Guilford College
Greensboro, NC 27410

Back issues may be purchased by sending $US 15.00 per volume to the editorial office.

The *Journal of Undergraduate Research in Physics* is published by the Physics Department of Guilford College for the American Institute of Physics and the Society of Physics. **ISSN 0731-3764**

GOTHIC CATHEDRALS, EXPERIMENTAL PHYSICS AND PUBLISHING

When you travel through central Europe, one spectacular sights that are hard to miss are the amazing monuments that were built more than 500 years ago out of stone, mortar and the sweat and blood of countless unknown people. The persons who designed and directed the construction of these Gothic cathedrals must have been either excellent experimental physicists or extremely lucky to keep those structures from succumbing to the relentless working of time and gravity. This weak but universal force tries to flatten out the high peaks and fill in the low valleys of the world rather than maintain high vaults and spindly columns.

The age of the 'cathedral building crusades' [1] began shortly after the turn of the 11th century, just after the completion of the first of the 'religious crusades' and lasted through the 15th century, interrupted, as in the case of modern physics, by wars and lack of funding. It started in the central European region known as the 'Isle de France', moved on to the Germanic countries and finally to Spain. [2]

The late medieval era must have been a very exciting time. As is currently happening, the citizens of Europe threw off the stifling cloak of the feudal barons, kings and church. It was a time of relative freedom for individuals. The concept of a free man was revived, but unlike the Greek times, a few medieval people did not grab freedom at the expense of a large number of slaves. Common people of humble origins could become bishops and even cathedral builders.

This robust era was closed by a group of people who 're-discovered the classic world'. The renaissance, as this time has been dubbed by the art historians, saw the artist and builder, such as Michelangelo, become an almost slave to the secular and religious barons. These people, much infatuated with their so called 're-discovery ', looked at the works of the previous age, perhaps were jealous, and decided to defame them. They dubbed the previous era with the insulting name 'Gothic', in remembrance of the tribes of barbarians that ran over the beautiful (but rather decayed) classical Roman Empire. Unfortunately, they were not just satisfied to call the medieval works bad names, they also proceeded to destroy much of what was done during that time. As a consequence of the thoughtless actions of the people of the renaissance, there is not much left, outside of pieces of art, a few books and some stunning architectural structures, for us to find out about the builder/physicists who created and lived in this time of freedom and growth in Europe.

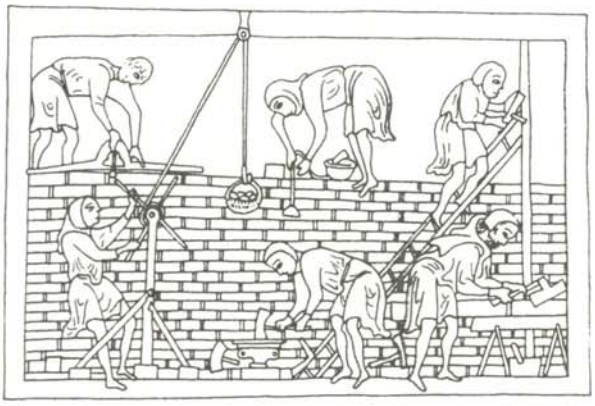

Sketch of an illumination from a manuscript from 1250 showing masons constructing the wall of a Gothic church. [8] The original is in Dublin Trinity College.

There is a significant contrast between the art and writings that are left from Gothic times and the remaining buildings that still evoke feelings of awe and wonderment in the mind of the visitor. The art and writings to have few connections to the physically real world, the realm in which physicists play. The art shows no three dimensional character, relative size is of vanishing importance and chronological time plays no role in determining the sequence of events. Likewise, the written works show a disrespect for ordering things in time. The concept of factual reporting of historical events is missing. I would like to call these sort of artifacts Gothic 'flat works'. Most of what we learn in the college or university about the Gothic times has to do with the 'flat works'. The form and content of the 'flat works' were determined by the current philosophy and theology . They did not have to stand the test of truth known as nature.

The buildings, on the other hand, are a realization of the creative drive of individuals with an incredible working knowledge of all three dimensions of the physically real world. The soaring heights of the vaults (often up to 40 m) and seemingly light supports (length to diameter ratios > 10) [3] of the cathedrals are sufficient rea-

son to believe that someone at this time imagined in three dimensions, had a practical working knowledge of physics and a clear understanding of how one must sequence events to maintain a building program that might last 25 to 300 years. There is significant evidence that the design of the design was determined not by theology or 'sacred geometry', but by how one had to construct the scaffolding and falsework necessary to actually build the high vaults. [4]

It is clear that the builders of the cathedrals could not have used Newton's methods, published in 1645, to design the cathedrals. What ever calculations they did, if ever written down, are now gone. Paper was very expensive, used only by the very rich or the monks in the abbeys. The parchment record shows that the learned knew little about mathematics. In the 11th century, the European ecclesiastical scholars could not prove even simple theorems about geometry. The tools and illuminated manuscripts that are left from the medieval times show that the builders had a working knowledge of geometry, trigonometry and maybe even some algebra.[5]

With no written record left, how does one find out about the physics that the cathedral builders must have developed? Fortunately, as in case of geology, we are left with the results of the original builders. Instead of a fossil record, we have a record of cut stone and mortar which I would call the fabric record. [6] Despite the Victorian renovations and renaissance destruction, the fabric record is only slightly eroded. In the spirit of geology, what can we learn about the state of physics (how people modeled the actions of nature) in the Gothic times from examination of the fabric record?

The vertical sections of the cathedrals show that some of the builders had a good intuitive knowledge of vectors and forces. A good example is the cathedral at Bourges. The daringly different buttressing design used by the original builder of the choir is similar to what one would design today using Newton's laws and computers. [7] The rubble fill on top of the ribbed vaulting shows that the builders understood the difference between force and pressure.

This early gothic physicist, the original builder of Bourges Cathedral, did not leave a permanent record of the justifications of his design system. A second builder, just 30 years later, who finished the nave, modified the buttressing system to agree with the 'accepted way' and in the process produced a structurally less sound support system. He fell into the trap of making reality fit the theory. It is sad that there was no Journal of Gothic Design Theory to record the ideas and design algorithms of the first builder.

As one examines the various bays in the cathedrals, the modifications in design make one believe that the Gothic physicists were experimentalists. The church building itself was their laboratory. They modified their understanding of how nature operates from the failures and cracking of the parts they just finished building rather than predictions using numerical models.

The fabric record tells us that experimental physics was flourishing during the Gothic times. Today we do not know the clever thoughts and creative ideas of the Gothic physicists because they did not write down what they discovered. All that they knew had to be rediscovered by someone else. The profound lesson one learns from a study of the building of the Gothic Cathedrals is the necessary role publication plays in the advancement of the frontiers of physics.

1. Jean Gimpel, The Cathedral Builders, Translated from the French edition by Teresa Waugh, The Cresset Library, London, 1983.

2. John Harvey, The Gothic World 1100 - 1600, Harper and Row, New York, 1969.

3. Robert Mark, Experiments in Gothic Structure, The MIT Press, Cambridge, 1982.

4. John Fltchen, The Construction of Gothic Cathedrals, A Study of Medieval Vault Erection, The University of Chicago Press, Chicago, 1961.

5. Marie-Jeanne Geyer, Ed., Les Batisseurs Des Cathedrales Gothiques, Editions Les Musees de la Ville de Strasbourg, 1989.

6. Fabric is the old English word used to describe the shell of the church, as contrasted to the altars, statues etc. that make up the inside of the church.

7. M Wolfe and R. Mark, 'Gothic Cathedral Buttressing, the Experiment at Bourges and its Influence', J. Soc. Arch. Historians., 33, 1974 pp. 17-26.

8. G. Binding and N. Nussbaum, Der millelarlterliche Baubetried mördlich der Alpen in zeitgenössischen Darstellungen, Wissenschaftliche Buchgesellschaft, Darmstadt, 1978

THE MAGNETOPHONON EFFECT IN n-InSb

Robin E. Barber *
Department of Physics
The University of North Texas
Denton, TX 76203

ABSTRACT

The magnetophonon effect has been used to determine the effective mass of the conduction band electrons at different temperatures in n-type InSb. The results were obtained using the two-band model and comparisons are made with the results of other authors.

INTRODUCTION

One of the most useful parameters in the characterization of semiconductors is the effective mass. This value tells much about the band structure and the transport properties of the semiconductor. There are several ways to measure the effective mass. The most common method is using cyclotron resonance where a photon is used to excite an energy level that is produced by the motion of the charge carriers in the semiconductor when it is placed in a magnetic field. [1] The magnetophonon effect is produced in a similar fashion, but phonons, which naturally exist within the semiconductor, are used instead of photons to excite the energy level. This means that the same results can be produced without the use of a light source.

This paper reports the effective mass values of the conduction band edge electrons at temperatures between 40K and 160K in n-type InSb found by the use of the magnetophonon effect. The values are then compared with other published results and the predictions of theory.

THEORY

When atoms are brought close together, as in a semiconductor, the inter-atomic forces between them result in the creation of energy bands. The existence of the band structure can be understood in the following way. Each individual atom has one or two degenerate electrons is each of its occupied energy levels. When the two atoms are brought in close proximity to each other, the degenerate levels are split into two separate levels as predicted by the Pauli exclusion principle.

When this model is expanded into N atoms, where N is very large, each degenerate level splits into N closely spaced levels or bands due to the interaction of the atoms with each other. The energy spacing between these levels is dependent upon the inter-atomic spacing within the semiconductor crystal.

Robin Barber graduated from the University of North Texas in August, 1989 with a BS in physics and a BA in computer science. Presently, she is employed by Bioserve Space Technologies while working on a Ph.D. in aerospace engineering at the University of Colorado at Bolder.

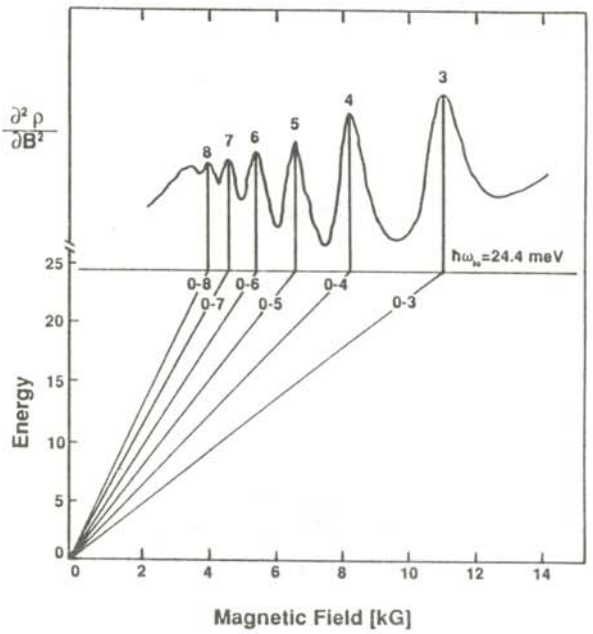

Figure 1
The bottom half of the figure shows the relationship between the Landau energies and the applied magnetic field. The upper part shows an idealized spectrum of the magnetophonon peaks for a phonon energy of 24.4 meV.

If a free electron is placed in a magnetic field, it will move in the helical motion described by the Lorentz force. If the magnetic field is defined to be in the z direction, the circular motion of the electron is in the plane perpendicular to the z direction. When a magnetic field is applied to a semiconductor, it quantizes the allowed energies into a series of sub-bands known as Landau levels. The allowed energies of these Landau levels are given by:[2]

$$E = \left(n + \frac{1}{2}\right) \frac{h}{2\pi} \omega_c + \frac{\left(\frac{h}{2\pi}\right)^2 k_z^2}{2 m_o^*} \qquad (1)$$

where m_o^* is the conduction band edge effective mass, n is the Landau level number, k_z is the size of the wave vector in the z direction and ω_c is the cyclotron resonance frequency given by:

$$\omega_c = \frac{n e B}{m^*} \qquad (2)$$

where e is the charge on the electron and m* is the effective mass of the electron. In addition, the scattering lifetime of the electrons, τ, must be large enough such that: [2]

$$\left(\frac{h}{2\pi}\right) \omega_c \geq \frac{\left(\frac{h}{2\pi}\right)}{\tau} \qquad (3)$$

This is known as the cyclotron resonance condition. It stipulates that for Landau levels to exist, the electrons must complete a large part of a cyclotron orbit before they are scattered. If the lifetime of the electrons is too small, the scattering is very probable and the Landau levels are unresolved.

The magnetophonon effect occurs when the electrons in the conduction band are resonantly scattered between the Landau levels close to $k_z = 0$ by longitudinal optical frequency phonons. By controlling the strength of the magnetic field applied to the semiconductor, the energy spacing between the Landau levels can be varied and the effective mass of the electrons can be measured. Resonant scattering between Landau levels will happen only when:

$$n \left(\frac{h}{2\pi}\right) \omega_c = \left(\frac{h}{2\pi}\right) \omega_{lo} \qquad (4)$$

is satisfied. This is the second condition necessary for the magnetophonon effect to take place. Substituting Equation 4 into Equation 2 yields:

$$\omega_{lo} = \frac{n e B}{m^*} \qquad (5)$$

When resonant scattering occurs between bands, the resistance of the sample is at a maximum. This resistance shows a pattern oscillating peaks

as the magnetic field is changed, showing how much scattering is occurring between bands as they are split farther apart by the increasing magnetic field.

The lower part of Figure 1 shows how the conduction band Landau levels split as the applied magnetic field increases. The labels represent the quantum numbers of the Landau Levels participating in the electron scattering that give rise to the observed magnetophonon resonance. Since the lowest lying Landau level contains the largest population of electrons, the strongest transitions are those due to scattering from the n = 0 level. The upper part of Figure 1 portrays the resonant oscillations that occur as the magnetic field increases. The second derivative of the magnetoresistance is shown because the lock-in amplifier must be set accordingly during the experiment for accuracy.

The temperature dependence of the effective mass can be explained by electron-phonon interactions. As phonons travel through a semiconductor, they are absorbed and/or emitted by the electrons in the bands with quantized amounts of energy. The phonon population increases with rising temperature, and since the effective mass is inversely proportional to the phonon energy, the effective mass decreases with an increase in temperature. [3] The energy gap between the conduction band and the valence band as function of temperature is given by the Varshni equation: [4]

$$E_g(T) = E_g(0) - \frac{\alpha T^2}{\beta + T} \qquad (6)$$

where $E_g(0)$ is the energy gap at 0K, T is the absolute temperature, and the constants α and β are 0.6 MeV/K and 500K respectively. [5]

The two band model of a semiconductor produces an accurate value for the effective mass by using the energy gap to describe the difference in energy between the conduction and valence band energies. The two band model predicts the electron energy E as: [6]

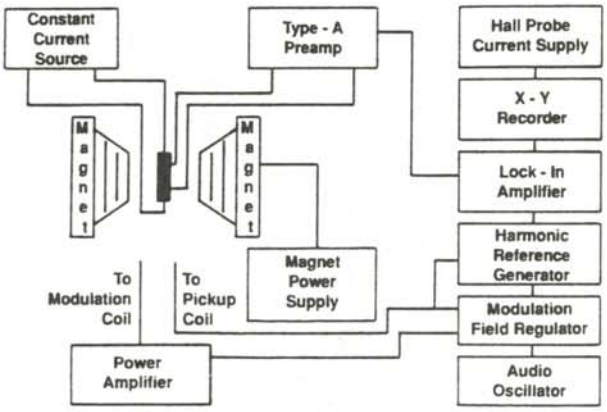

Figure 2
Experimental configuration used in performing this experiment.

$$E = -\frac{1}{2} E_g \pm \left[\left(\frac{E_g}{2} \right)^2 + E_g \frac{\left\{ \frac{h}{2\pi} \right\}^2 k^2}{2 m_o^*} \right]^{\frac{1}{2}} \qquad (7)$$

where m_o^* is the effective mass of the electron at the bottom of the conduction band. The effective mass of the electrons in the semiconductor is given by :[6]

$$\frac{1}{m^*} = \frac{1}{\left(\frac{h}{2\pi} \right)^2 k} \left\{ \frac{\partial E}{\partial k} \right\} \qquad (8)$$

Taking the derivative of Equation 7 and substituting it into equation 8 yields:

$$m_o^* = \frac{m^*}{1 + \left(\frac{2E}{E_g} \right)} \qquad (9)$$

which relates the effective mass of the electrons to the effective mass of the conduction band edge electrons. This model includes the nonparabolicity of the bands, which predicts a dependence of the effective mass on energy.

An experimental value of m* can be determined using Equation 5 by plotting measured values B

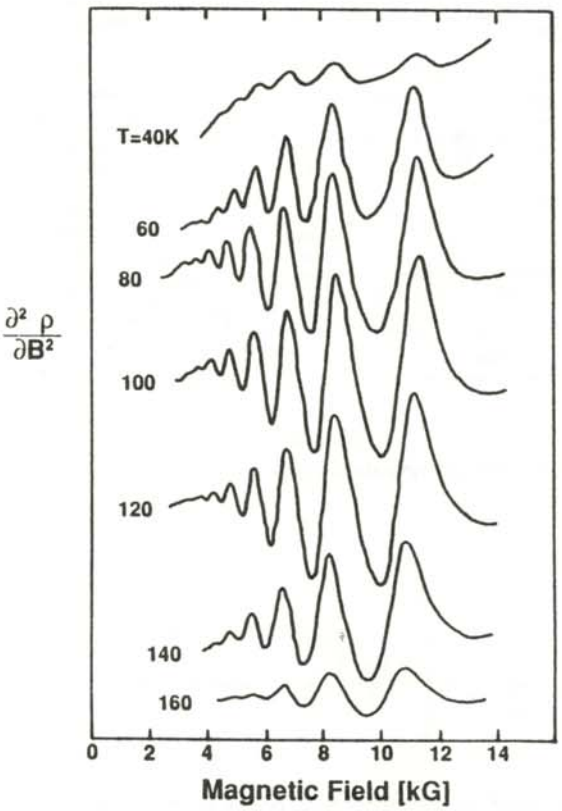

Figure 3
Recorded data at several different temperatures. Note the incrase in amplitude of the oscillations in the center region of the temperature range

vs n. The slope of this line is:

$$\text{slope} = \frac{\omega_{lo}\, m^*}{e} \qquad (10)$$

where the value for ω_{lo} for the longitudinal optical frequency phonons is a known quantity determined by the conditions of the experiment. Equation 9 then can be used to relate this value of m_o*. The value of E_g at each particular energy if found using Equation 6. Since the measured effective mass is an average of its values in the two Landau levels participating in the resonant scattering process, the electron energy can be found using:

$$E = \frac{1}{2}\left(\frac{h}{2\pi}\right)\omega_{lo} + \frac{1}{2}\left(\frac{h}{2\pi}\right)\omega_c \qquad (11)$$

EXPERIMENTAL METHODS

A schematic diagram of the experimental apparatus is shown in Figure 2. The n-type InSb sample was placed in a magnetic field monitored by a Hall probe. A transverse constant current of (1.50 ± 0.01) mA was run through the sample to measure the resistance.

The sample was driven by a constant current source. This provided a constant voltage/ resistance across the source. The voltage was measured by an oscilloscope. The oscilloscope was set to carry a 43 Hz modulation if the sample has a non-zero magnetoresistance. This signal then was fed into a lock-in amplifier which demodulated it to a dc voltage. The lock-in amplifier was set to the frequency of the second harmonic (86 Hz) making its output proportional to the second derivative of the magnetoresistance.[7]

Data were recorded at temperatures ranging from 40K to 160 K in intervals of about 5K up to 80 K and then in about 10K intervals up to 160. The magnetic field was varied up to 14 kGauss

RESULTS

Figure 3 shows raw data taken at several temperatures. Each trace follows the general shape predicted in the upper part of Figure 1. The interesting feature to notice is the amplitude of the peaks at the boundaries of the temperature range as compared to the amplitudes at the center of the range. Below about 40K, the population of the phonons is low, hence only weak oscillations are observed. Above 160K, the Landau levels become unresolved due to the large scattering because the lifetime of the cyclotron oscillations is not long enough.

The value of the effective mass of the electron was extracted by finding the magnetic field at the maxima of the oscillatory peaks and plotting the

inverse of those values vs. the Landau level number at each temperature. This slope of this line was placed in Equation 10 along with the value of $\omega_{lo} = (3.71 \pm .03) \times 10^{13}$ Hz. to determine m*. The conduction band edge effective mass m_o* was calculated from this experimental value of m* and the results of the two-band model given by Equation (9).

Figure 4 shows the results of this experiment and those of other authors. The data of the other authors [9,10] are shown along with the theoretical predictions [11] which take into account the influence of the higher order bands. The data from this experiment show a decrease in the effective mass with temperature, similar to that of the other magnetophonon experiments and the theoretical predictions.

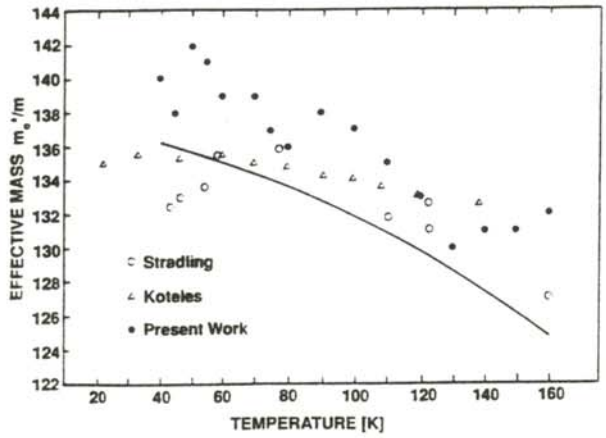

Figure 4
Effective mass vs. temperature. The line drawn is the prediction of the theory [11].

ACKNOWLEDGEMENTS

The author wishes to thank Reza Loloee for his help in preparing the experimental apparatus. She also wishes to extend thanks to Dr. Chris Littler for his time and guidance while making this project possible.

REFERENCES

* Present Address: Bioserve Space Technologies, Department of Aerospace Engineering, Box 429, University of Colorado, Boulder, Boulder, CO 80309-0429

1) E.J. Johnson and D.H. Dickey, Phys. Rev. B, 1, 2676, 1970.

2) D. Long, Energy Bands in Semiconductors, (John Wiley and Sons, 1968), pp. 68-69.

3) *Ibid.*, pp 50-51.

4) Y.P. Varshni, Physica, 34, 149, 1967.

5) C.L.Littler and D.G. Seiler, Appl. Phys. Lett, 46, 986, 1985.

6) W. Zawadzki, New Developments in Semiconductors, ed. Wallace, et.al., (Noordhoff International Publishing, 1973), pp. 454-455.

7) H. Kahlert and D.G. Seiler, Rev. Sc. Instrum. 48, 1017, 1977.

8) M.W. Goodwin and D.G. Seiler, Phys. Rev. B, 27, 3451, 1983.

9) E.S. Koteles and W.R. Datars, Phys. Rev. B, 9, 568, 1974.

10) R.A. Stradling and R.A.Wood, J. Phys. C: Solid St. Phys., 3, L94, 1970.

11) E.O. Kane, J. Phys. Chem. Solids, 1, 249, 1957.

FACULTY SPONSOR

Dr. Chris Littler
Department of Physics
University of North Texas
Denton, TX 76203

OPTICAL ABSORPTION OF SUNGLASS LENSES AND SUNSCREENS

Urszula Tajchman*
Department of Physics
West Virginia University
Morgantown, WV 26506

ABSTRACT

A spectrophotometer was used to measure the optical absorption of various sunglass lenses and sunscreens in the visible and ultraviolet regions. We found that all glasses tested absorb ultraviolet wavelengths which can cause cataracts. Polarizing lenses were found more efficient in protecting the eye against the more harmful shorter wavelengths of visible light which cause retinal damage. We found that sunscreens with the same SPF values may not have the same absorption spectra and that lotions may have a higher absorption coefficient than oils in the visible spectral range.

INTRODUCTION

The sun can be thought of as a blackbody at approximately 5900K. A blackbody emits radiation according to Planck's equation:

$$I(\lambda,T) = \frac{hc^2}{\lambda^5} \frac{1}{e^{\frac{hc}{k\lambda T}} - 1} , \qquad (1)$$

where I is the intensity of the radiation at wavelength λ, T is the temperature and h and k are Planck's and Boltzmann's constants respectively. A plot of intensity versus wavelength for the sun shows that most of the radiation we receive is in the visible and near infrared ranges with a maximum intensity at 475 nm. The radiation from the sun, however, is absorbed by the molecules in the atmosphere, producing a different solar spectrum than this on the surface of the earth. This spectrum measured on earth varies with factors such as: time of year; solar elevation; cloudiness and pollution in the atmosphere. For example, the small angle of the sun in the winter results in wavelengths below 310 nm being absorbed by the atmosphere. [1] When the sun is at an elevation of 30°, the distance through the atmosphere that solar radiation must travel to reach the earth is twice that when the sun is at the zenith. The amount of radiation reaching the earth is usually decreased by the presence of clouds. However, reflection from scattered cumuli can actually increase the amount of ultraviolet light reaching us. [2]

Scattering by gas molecules in the atmosphere occurs for shorter wavelengths and is more important in the ultraviolet region. Scattering by larger molecules and dust particles in the air oc-

---

Urszula is currently a first year medical student at Johns Hopkins School of Medicine. She did this work while a senior. In addition to her graduate studies, she finds time to plany in a rock band.

curs for longer wavelengths. Such scattering is more prevalent in city areas with pollution. [3] In general, half of the radiation reaching us comes directly from the sun and half is diffusively scattered. [2] The amount of radiation reaching our bodies also depends upon the reflectance of our surroundings. For example, snow reflects 85% of diffuse UV-B radiation (280 - 315 nm), while water may only reflect 5%.

These are only a few of the factors that affect the amount of light of different wavelengths that reach us. The large number of different interactions that take place as sunlight passes through the atmosphere makes it difficult to predict how much radiation of a certain wavelength will be incident on our skin or eyes at any given time.

Effects of Radiation on the Eye

Some of the adverse effects of radiation on the eye, including those that motivated this experiment are shown in Figure 1.

The cornea is the part of the eye that is exposed directly to the outside. The aqueous fluid behind the cornea is mainly water. Both protect the lens of the eye from infrared radiation. [4] The anterior portion of the eye absorbs far-ultraviolet and far-infrared light. Excess exposure to this type of light can be harmful to the cornea and possibly to the lens. The lens also absorbs a great deal of ultraviolet light of wavelengths greater than 300 nm.

Cataracts occur when the normally clear lens becomes opaque, inhibiting the light rays from reaching the retina, leading to blurred vision. Cataracts can be caused by the absorption of ultraviolet light by the lens, causing a breakdown of the chemical structure of the lens. [4]. For this reason, sunglasses should filter out ultraviolet light.

The retina consists of complex nerve cells, including photoreceptors. Immediately posterior to these is the retinal pigment epithelium (RPE). Normal function of the RPE is important for retinal metabolism and photochemistry and thus for normal vision. Because most absorption of the visible and infrared light occurs in the retina, these wavelengths cause the most retinal damage. The 'retinal hazard region' is 400 - 1400 nm.

Damage to the retina can be understood by examining the interaction of radiation with matter. Absorption of the incoming radiation by the molecules in the retina is governed by quantum restrictions. Photons with energies in the near

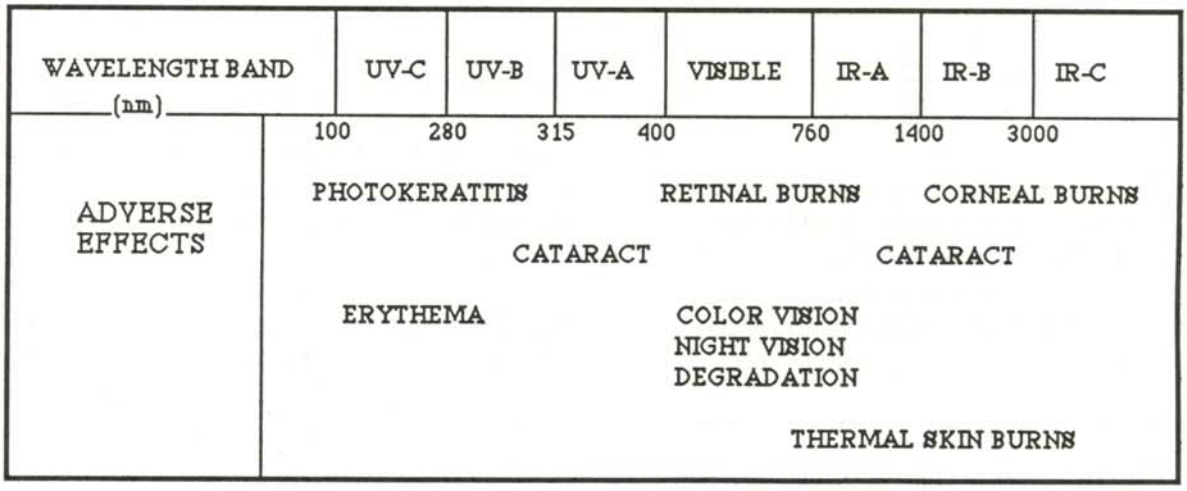

Figure 1
A list of some of the adverse effects of radiation on the human body that were a motivation for this experiment.

infrared and low-energy visible regions correspond to allowed vibrational states of the molecules [5]. The absorption of these photons by the retina and RPE leads to a temperature increase in the material, resulting in injury from protein denaturation. A temperature increase of 15-20 C causes thermal retinal injury. [4,5]

On the other hand, high-energy visible and ultraviolet photons cause damage by a photochemical process. The energy of these photons correspond to energy differences between excited and ground states of electrons in the retinal molecules. The photons are absorbed, exciting the electrons . They return to the ground state , dissipating their energy in a way such that the photochemical damage can spread from one molecule to another in a chain like fashion. [5] This process results in retinal lesions in a very short time. When the sun is at the zenith and there are no clouds in the sky, a lesion can be produced in less than one minute if one is staring directly at the sun. [5]. In general, experiments show that the damage-threshold irradiance of the retina increases with wavelength, and that the severity of retinal lesions increases with photon energy. [4,5] Therefore, sunglasses should be made to absorb blue and violet light as well as the infrared.

Effects of Radiation on the Skin

Solar radiation also has physiological effects on the skin. The wavelengths that cause the greatest effect are shorter than those used in this experiment. Exposure to ultraviolet light has been connected with skin aging and cancer because the maximum absorption of light by nucleic acids occurs at 260 nm.

Another common result of radiation on the skin is erythema or sunburn. Wavelengths near 297 nm cause the greatest erythema. [6] Burning occurs when the absorption of ultraviolet waves causes injury to the skin, which the produces a vasodilator that enlarges the dermis vessels, making the skin look red. The skin protects itself from erythema by three methods. There can be an increased growth of skin which results in less harmful light reaching the lower skin layers.[7] Another method is an increased production of melanin granules which reach the outside of the skin in 3-4 weeks. [6] The third method is the formation of photo-oxidative melanin (which has an absorption peak at 350 nm), which occurs within one hour of the stimulation by sunlight. [7] Melanin can be darkened upon exposure to wavelengths in the range 330 - 400 nm. [2]

The skin can also be protected by placing on top of the skin substances which absorb the harmful radiation before it has a chance to do damage. Sunscreens are classified by the 'Sun Protection Factor' or SPF. A SPF2 means that the exposure time to cause damage to the skin with the sunscreen applied is twice that with no sunscreen applied.

The best-known sunscreen agent is para-amino benzoic acid or PABA. Its maximum absorption is at 266 nm. Other screening agents are Ethylhexyl p-methoxycinnamate which has an absorption peak at 308 nm and oxybenzone which absorbs best at 290 nm. [8]

THE EXPERIMENT

The absorption data were gathered using a Cary 14 spectrophotometer. The Cary 14 uses a prism as a monochromator. The prism is rotated to vary the wavelength of light which is used for the absorption studies. The beam is split into two, one passing through a sample compartment and the other through the reference compartment. The instrument compares the intensities of the two light beams to determine how much light is absorbed by the sample at that particular wavelength.

The optical density, OD, of the sample can be determined by:

$$OD = \log \{I_0 / I\} , \qquad (2)$$

where I_0 is the intensity of the incident light and I is the intensity transmitted through the sample. Because different physical thicknesses of the same material absorb different amounts of light, the absorption coefficient, K, provides a better measure of absorption by different materials.

Lenses		
a	J.C. Penny	Lot SD646
b	J.C. Penny	Lot DC609
c	J.C. Penny	Lot DC638
d	J.C. Penny	Lot DC608
e	J.C. Penny	Lot DC612
f	J.C. Penny	Lot DC617
g	J.C. Penny (polarizing)	Lot DC629
h	Ray Ban	

Sunscreens	
1	Hills
2	Sum'er Tan
oil	Sum'er Tan

Table 1
A list of the lenses and sunscreens used in the experiment.

The absorption coefficient is given by:

$$K = 2.303\ (OD) / d, \qquad (3)$$

where d is the thickness of material which absorbed the light.[9]

For this experiment, a special sample holder was constructed to hold the lenses so that a curved lens would be situated perpendicular to the incoming light beam. Glass test tubes were used to hold the sunscreens.

Table 1 lists samples the whose optical absorption was measured in the range 360- 660 nm. The absorption coefficients were determined at wavelength intervals of 5 nm. using Equation 3.

Eight sunglass lenses were tested. The reference for these measurements was a pair of untinted prescription reading glasses. Two types of lotions and one oil were used in the sunscreen tests. Empty test tubes were used as the references for the latter measurements.

RESULTS

Plots of K versus wavelength for the lenses tested are shown in Figure 2. The absorption spectra have peaks at various positions in the visible region. The absorption of most of the lenses decreases at the shorter end of the visible spectrum, where the potential for damage to the retina is greatest. All of the lenses show sharply increasing absorption in the ultraviolet region. Lenses c and g, however, show absorption coefficients that, on the average, increase with decreasing wavelength. The absorption coefficient of the untinted reading glasses is zero in the visible range with a sharp increase beginning at 360 nm. Table 2 shows a summary of the results. These data show that only the polarizing lens consistently transmits less than 10% of the incoming light.

Errors in wavelength readings or positioning of the lenses in the sample holder are not significant enough to change the overall results of this experiment. For example, a 20° deviation from the perpendicular for a lens of thickness 0.16 cm would result in a 6% error in the calculated value of K.

Although all three sunscreens were marked 'SPF 4', the three corresponding absorption profiles are significantly different. Plots of K versus wavelength for the sunscreens tested are

Lens	λ (cm)	Effect	K (cm^{-1})	OD (d=.16cm)	% Transmit
(all)	360	cataract	>40	---	0
d	400	retinal	4.6	.32	47.9
g		damage	40.0	2.78	.2
h		-violet	10.0	.69	20.4
d	460	retinal	10.7	.74	18.2
g		damage	18.8	1.31	4.9
h		-blue	8.7	.60	25.1
d	570	retinal	7.0	.49	32.4
g		damage	18.2	1.26	5.5
h		-yellow	8.2	.57	26.9
d	650	retinal	4.9	.34	45.7
g		damage	16.6	1.15	7.1
h		-red	10.1	.70	20.0

Table 2
Results of the lens portion of the experiment. Approximate values of K were found from Figure 2. The lens identifications can be found in Table 1.

shown in Figure 3. Both lotions absorb a greater amount than the oil.

The absorption of the lotions increases gradually with decreasing wavelength until the ultraviolet region, where there is a sharp increase in absorption. On the other hand, the absorption by the oil decreases with wavelength in the visible region, but shows the same sharp increase in the ultraviolet.

DISCUSSION OF RESULTS

Table 2 shows that ultraviolet light is absorbed by all the the sunglass lenses. This occurs because the band gap energy of the electrons in the glass corresponds to the photon energy in the ultraviolet region.

Several of the lenses transmit up to 50% of the light in the region 380-430 nm. In a previous study [10], it was found that many commercially available sunglasses have UV and IR windows that allow passage of harmful light. This is dangerous to the wearer because any attenuation of

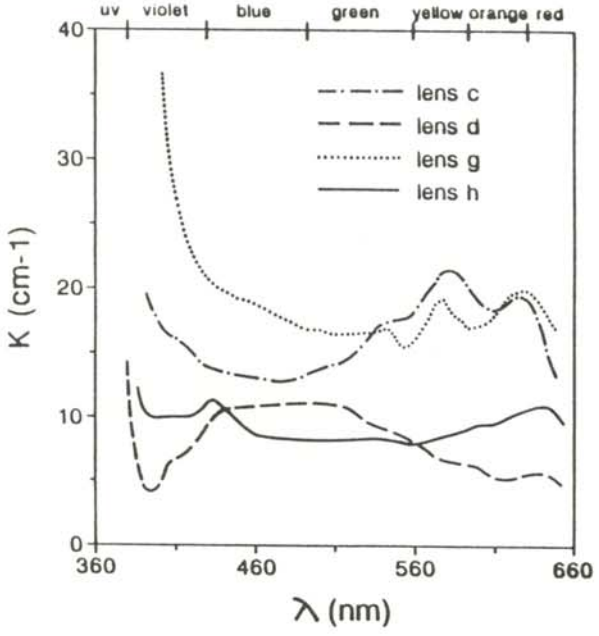

Figure 2
Absorption coefficient as a function of wavelength for sunglass lenses

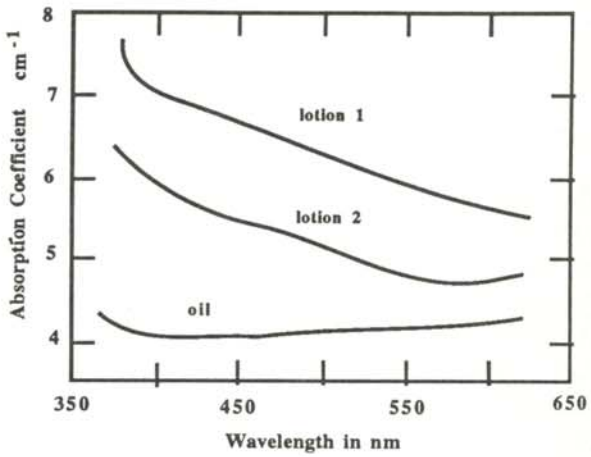

Figure 3
Absorption coefficient as a function of wavelength for sunscreens.

visible light results in the dilation of the pupil. If UV and IR windows are present, more harmful radiation can enter the eye than if sunglasses were not worn.

It is important that sunglasses absorb high-energy visible light. The polarizing lens seems to be the most effective in this region. A 0.16 cm thick lens of this material transmits only 5% of the high-energy visible light incident on it. Some of the more expensive sunglasses (e.g. lens h) do not show especially strong absorption in the short wavelength regions. For low-energy visible light, the polarizing lens we tested is again the most effective absorber while the expensive lens has a relatively low absorption coefficient.

Of the lenses tested in this experiment, the polarizing lens seems the safest for the eye. This might be expected as these lenses absorb all components of light except those oscillating in a certain direction. This absorption is independent of wavelength, so a substantial amount of light of all wavelengths will not be able to reach the eye. However, other experiments found that some polarizing lenses permit as much as 80% transmission of IR radiation.[11]

For the lenses tested, absorption does not seem

to be a function of lens color but of the material of which the lens was made and the impurities added to it. This is in agreement with previous experiments which have found no correlation between absorption and lens color or cost.[10,12]

The optical absorption by sunscreens is more difficult to analyze because of the uncertain penetration of the sunscreens into different layers of the skin and the reflection of light by the skin. The ideal sunscreen would have strong absorption in the regions which have the greatest adverse effects (266 nm and 300 nm regions) and less absorption in the shorter wavelength visible region which causes melanin production and darkening. The oil that was tested seems to fit this last criterion the best even though its absorption in the ultraviolet region may be lower than that of the lotions.

ACKNOWLEDGMENTS

This project was suggested by Dr. M.S. Seehra and Dr. V.K. Raju. Most of the lenses were provided by Dr. Raju. The optical studies were carried out in the laboratory of Dr. Seehra, who also provided technical guidance. Dr. G. Thevar gave some assistance in graphing and Dr. S.J. Tajchman provided some background information. The author also wishes to thank Dr. M. Koepke for his help in preparing the manuscript.

REFERENCES

* Present Address: The Johns Hopkins School of Medicine, Baltimore, MD 21205.

1. J.R. Cameron and J.G. Skofronick, Medical Physics, Wiley-Interscience, New York, 1978, pp. 312-329.

2. D.D. Houghton, ed., Handbook of Applied Meteorology, Wiley-Interscience, New York, 1985, pp. 778-795.

3. I. Dirmhirn, Das Strahlungfeld im Lebensraum, Akademische Verlagsgesellschaft, Frankfurt am Main, 1964.

4. D. Sliney and M. Wolbarscht, Safety with Lasers and Other Optical Sources, Plenum Press, New York, 1982.

5. R.N. Young, Surv. of Opthalmol., 32, 252, 1988.

6. R.K. Hobbie, Intermediate Physics for Medicine and Biology, Wiley-Interscience, New York, 1985.

7. R.K. Clayton, Light and Living Matter: A Guide to the Study of Photobiology, Vol. 2, McGraw-Hill, New York, 1985.

8. M. Windholz, ed., Merk Index, 10th ed., Merk and Company, Inc., Rahway, NJ, 1983.

9. W.W. Kou and M.S. Seehra, Phys. Rev. B, 18, 7602, 1978.

10. W.J. Anderson and R.K.H. Gebel, Applied Optics, 16, 515, 1977

11. E.C. McCullough and G.D. Fullerton, Surv. of Opthalmol., 16, 1971.

12. B. Borgwardt, G.A. Fishman, and D.V. Meulen, Arch. Opthalmol., 99, 293, 1981.

FACULTY SPONSOR

Professor Mark. E. Koepke
Department of Physics
West Virginia University
Morgantown, WV 26506

CONSTRUCTION AND PERFORMANCE OF A FREE-STANDING WIRE GRID POLARIZER AT MILLIMETER WAVELENGTHS

James P. Schwonek
Massachusetts Institute of Technology
Cambridge, MA 02139

ABSTRACT

An inexpensive and simple method of constructing high quality wire grid polarizers suitable for use in millimeter wave optics is described. Criteria for evaluating their performance are presented and test conditions are described. Performance results are compared with those of a commercially available product.

INTRODUCTION

With millimeter wave radiation, one often encounters conditions similar to those found in optical wave propagation: the radiation frequently travels in the form of a plane linearly polarized transverse waves. The direction of polarization can be measured or selected with a polarization sensitive device. Because optical polarizers are generally unsuitable in the millimeter wave region, one must construct special devices for this purpose. Free standing wire grids, composed of a parallel array of fine wires have been utilized with excellent results. [1,2,3,4]

James is a senior majoring in Physics at MIT and has been working there as an undergraduate research assistant since 1987. He is planning to study experimental atomic physics in graduate school

Constructing such a grid presents a mechanical challenge because of the requirement for accurate alignment of wires that are spaced by no more than half a wavelength. This problem may be solved with the use of a commercial coil-winder, [2] but such an instrument is seldom found in the machine shop.

This paper describes a method of constructing a high quality wire grid polarizer designed for use at 256 GHz. The method can be extended to somewhat shorter wavelengths. Criteria for evaluating the performance of the grid are presented and the test conditions are described. Finally, the performance results are compared with those of a similar product available commercially.

THEORY

When electromagnetic radiation is normally incident upon an ideal polarizer, the component of the electric field parallel to the transmission axis

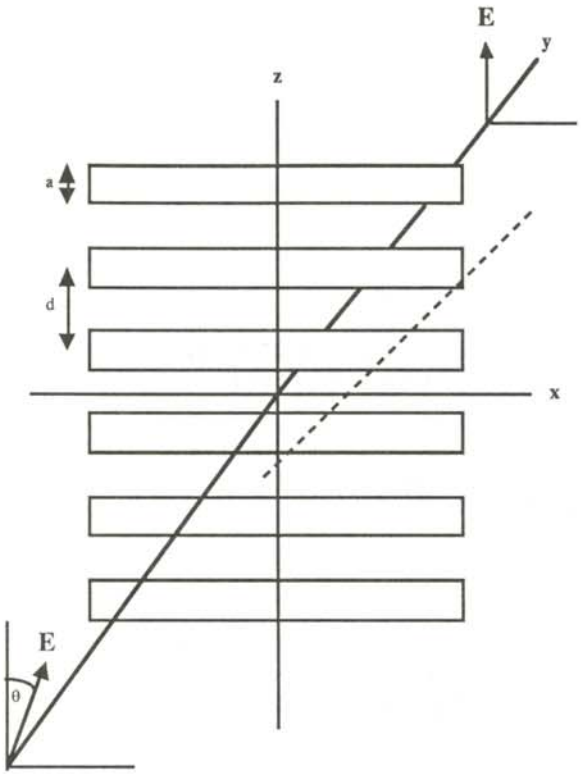

Figure 1
Linearly polarized radiation traveling in the y direction is normally incident upon a wire grid polarizer at y = 0. The grid has a wire thickness, a, and a wire spacing, d. The angle θ used in Equation 1 is defined as the angle between the incident polarization and the polarizer's transmission axis, z.

is unaffected, while the component perpendicular to this axis is extinguished. Thus, the amplitude of the electric field of the transmitted component varies as the cosine of the angle between the electric field and the axis of the polarizer. The power transmittance, T, is given by Malus' law : [5]

$$T(\theta) = I / I_o = \cos^2(\theta) , \qquad (1)$$

where I_o is the incident intensity, I is the intensity of the transmitted wave and θ is the angle between the incident electric field, **E**, and the polarizer's transmission axis as shown in Figure 1.

In the case of real polarizers, [6] however, this equation has to be modified to take into account losses and leakage effects. Malus' Law then becomes:

$$T(\theta) = k_1 \cos^2 \theta + k_2 \sin^2 \theta , \qquad (2)$$

where k_1 is the maximum transmittance and k_2 is the minimum transmittance. When $k_1 = 1$ and $k_2 = 0$, this expression is identical to Equation 1. The parameters k_1 and k_2 are more usefully expressed in terms of two experimentally convenient quantities: the extinction ratio, R_E and the degree of polarization , P.

$$R_E = \frac{k_1^2 + k_2^2}{2\, k_1\, k_2} , \qquad (3)$$

$$P = \frac{k_1 - k_2}{k_1 + k_2} . \qquad (4)$$

The complete solution for the scattering of electromagnetic radiation by parallel cylindrical conductors is long and complicated. Fortunately, the problem has been solved and graphs of reflectivity and trasmitivity for various wire diameters and spacings are available. [7] For our purposes, it is sufficient to note that if **E** is perpendicular to the wires and $d/\lambda < 0.35$, where d is the center to center spacing and λ is the wavelength, k_1 tends toward 1 as a/d approaches 0 (a is the diameter of the wire). Similarly, if **E** is parallel to the wires and $d/\lambda < 0.6$, then k_2 tends toward 0 as a/d approaches 1. For example, if $d/\lambda = 0.2$ and $a/d = 0.3$, then $k_1 = 0.98$ and $k_2 = 0.01$.

CONSTRUCTION PROCEDURES

The construction of the polarizers employs a technique described by Sentz, et. al. [3] They used a lathe to wrap tungsten wire around a jig mounted ring and 'epoxied' the wire directly to this mounting ring. However, this method did not provide adequate uniformity of spacing for our purposes. Consequently, this method was modified by wrapping 50.8 μm (0.002") tung-

sten wire around a rectangular aluminum jig with a center hole. After removing the jig from the lathe the grid was mounted to its ring. The jig was turned on a lathe at 12 rpm while the tungsten wire was fed from a spool on the carriage. [8]

Figure 2 is a schematic diagram of the wrapping procedure. Adhesive tape on the ends of the jig kept the wire from moving as it was being wrapped. The wire spacing was regulated by the longitudinal feed of the carriage. A wire guide mounted on the carriage kept the wrappings parallel and taut. [9] Wrapping a grid 7.5 cm long took approximately 3 hours.

After removing the jig from the lathe, a 6.35 cm outside diameter x 5.08 cm inside diameter brass ring was 'epoxied' [10] to the grids on each side of the jig. The 'epoxy' was allowed to set 3 hours at approximately 40C. The polarizers

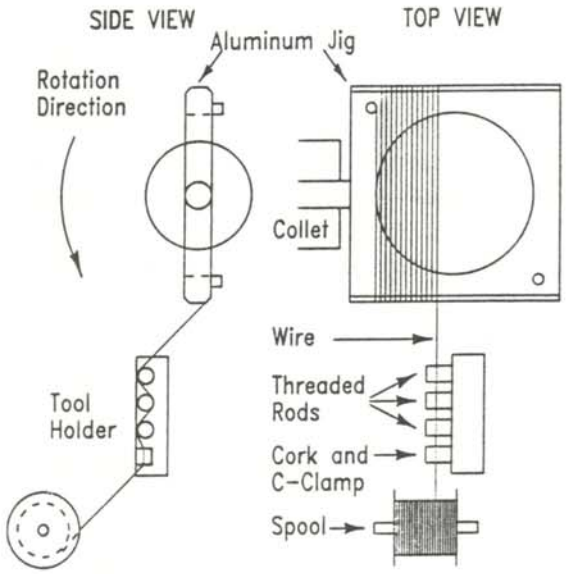

Figure 2
A schematic of the construction arrangement. The aluminum jig is secured to the collet of the lathe while the tool holder and tungsten wire spool travel along with the carriage. The wire travels from the spool through a piece of cork attached to the tool holder. Tension is maintained in the wire by compressing the cork with a C-Clamp. The wire runs through the threads of three rods which help to align the wire. The wire is tied to the jig by wrapping it around a screw.

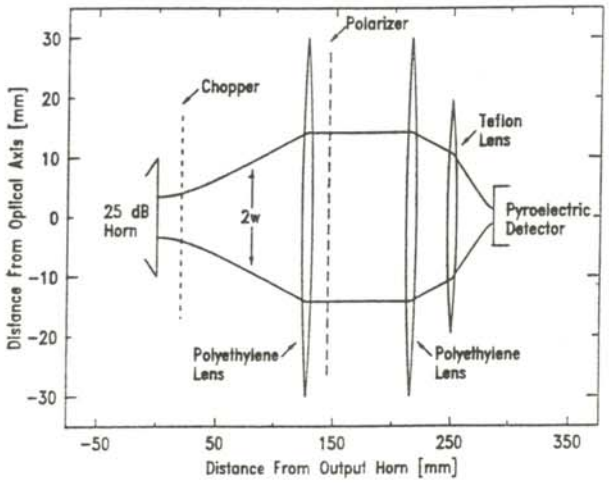

Figure 3
A schematic of the polarizer test. The millimeter radiation leaving the horn may be characterized by a beam diameter, 2w, that represents the distance from the optical axis at which the intensity of the radiation drops to $1/e^2$ of its center value

were removed from the jig by cutting the wires around each ring.

Our group discovered that the tungsten wires in the center of the ring experienced a slight loss of tension. This was probably due to the unequal thermal contraction between the brass and the tungsten which occurred after the 'epoxy' cured. To restore the tension, a second ring with a knife edge was constructed to press against the wires. After a good deal of experimentation with the construction technique, three polarizers were prepared. [11]

EXPERIMENTAL PROCEDURES

The spacing, d, of the wires was measured with a microscope to be 109 ± 10 μm. The gave a value of $d/\lambda = 0.093 \pm 0.014$ and $a/d = 0.47 \pm 0.07$. The theoretical values of k_1 and k_2 for these ratios are 0.97 and < 0.01 respectively. [12]

The performance of the polarizers was tested at 256.3 GHz. [13] The radiation was produced by a frequency-locked 64.075 GHz klystron whose output was quadrupled to yield the desired frequency. After passing through a 25 dB horn,

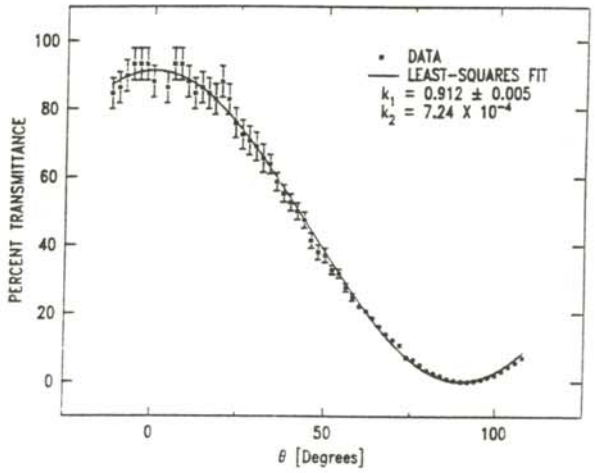

Figure 4
A plot of the transmission as a function of the polarizer angle θ. Equation 2 was fit to the data. The maximum transmittance, k_1, and the minimum transmittance, k_2, are shown.

the vertically polarized radiation entered the testing area shown schematically in Figure 3.

Since the wavelength of 1.17 mm was comparable to the size of the focusing elements, geometrical optics could not be used as a valid approximation for the propagation of the millimeter waves. [14] The 25 dB Horn produced a Gaussian beam profile. Beam-mode propagation theory was used to calculate the beam diameter as the beam propagated from the output horn through the various components to insure that the beam diameter remained well within the apertures of these components.[15] A plot of this beam diameter is superimposed upon the schematic diagram Figure 3.

Conventional quartz lenses cannot be used to focus millimeter wave radiation because their high index of refraction generates excessive reflections. Instead, specially constructed lenses of polyethylene and Teflon® were used. At 245 GHz, the index of refraction for quartz is 1.95 and its reflectivity is 10%. The corresponding figures for Teflon® are 1.46 and 4%. For polyethylene at 256 GHz $n \approx 1.5$ and the reflectivity = 6%. Because the lenses were large (diameter = 4 - 8 cm), it was also cost-effective to use Teflon® and polyethylene rather than quartz.

The millimeter wave power was measured using a pyroelectric detector. [16] The detector signal was fed into a lock-in amplifier whose reference signal was derived from an optical chopper. The chopper frequency was approximately 200 Hz, far from the 60 Hz line noise and its harmonics. The intensity of the radiation, $I(\theta)$, was first measured without the polarizer. After inserting the polarizer, the intensity was measured at 2° increments as the polarizer was rotated through a 120° range. The intensity without the polarizer was then measured again to insure that I_0 remained constant during the experiment. The ratio $I(\theta)/I_0$ is equivalent to $T(\theta)$ in Equation 2. The plot of T vs θ for one of the polarizers is shown in Figure 4.

ANALYSIS

To find k_1 and k_2, values from Equation 2 were fitted to the data for each polarizer using the Marquardt algorithm. [17]. The location of the minimum transmission coefficient, k_2, in Figure 4 was better defined than its maximum counterpart. This was probably due to the multiple reflections of the radiation between the detector body and the lenses interfering with the incident radiation. Such reflections could occur when there was a high transmission through the polarizer. In light of this, the algorithm varied k_1 while k_2 was kept constant at its measured value. The quantities R_E and P were then calculated from these coefficients. These results are summarized in Table 1.

SUMMARY

The polarizers performed well, having high extinction ratios and polarizing power. The theoretical model, however, predicted slightly higher maximum transmittance. The commercially available product ($d/\lambda = 0.078$ and $a/d = 0.25$) claimed at a frequency of 230 GHz values of $k_1 > 0.99$ and $k_2 < 0.01$. [18] The commercially available product also reported a higher maximum transmittance than our polarizers, but it was difficult to compare other specifications because the value of k_2 reported was an upper bound rather than a definite number. [19] The free

standing wire grid polarizers, however, were constructed at a small fraction of the commercial cost and yielded results comparable to the commercial product.

ACKNOWLEDGEMENTS

The author wishes to thank Scott Paine for his construction and technical assistance. Thanks also go to Pin Peter Chang and Robert Lutwak for their insights. Special thanks goes to Professor Daniel Kleppner for assisting with the manuscript preparation and to Frank Payne and Dave Taylor for their technical instruction. This research was supported by the MIT Undergraduate Research Opportunities Program and the National Science Foundation (PHY870650).

REFERENCES

1. G.J. Simonis and R.D. Felock, International Journal of Infrared and Millimeter Waves, 4, 3, 1983, p. 157.

2. A.E. Costley, K.H. Hursey, G.F. Neill and J.M. Ward, Journal of the Optical Society of America, 67, 7, 1977, p. 979.

3. A. Sentz, M. Pyee, C. Gastaud, J. Auvray and J.P. Letur, Review of Scientific Instruments, 49, 7, 1978, p. 926.

4. An alternative to free standing wire grids is to use a photoetched grid. Such a grid is mounted on a substrate that is transparent at the desired frequency. Free standing grids were chosen over the photoetched type because of the difficulty in finding a suitable substrate.

5. Hecht and Zajac, Optics, Addison-Wesley, Reading, MA, 1974, p. 226.

6. Melles Griot, Optics Guide 4, 1988, pp. 15-18.

#	1	2	3	Theory
k_1	0.917 ± 0.009	0.912 ± 0.005	0.966 ± 0.005	0.97
k_2	1.10×10^{-3}	7.24×10^{-4}	8.19×10^{-4}	<0.01
R_E	418 ± 10	630 ± 8	589 ± 7	>48.5
P	0.998 ± 0.013	0.998 ± 0.008	0.998 0.008	>0.980

Table 1
Tabulated results for the three polarizers. Quantities in the first column are as follows: k_1 = maximum transmittance, k_2 = minimum transmittance; R_E = extinction ratio and P = degree of polarization.

7. W. G. Chambers, A.E. Costley and J.T. Parker, International Journal of Infrared and Millimeter Waves, 9, 2, 1988, p. 157. The calculations assume infinite conductivity of the wire.

8. Although constant tension feeds were tried, the best result were obtained by winding directly from the spool using grommets on the spool axle to privide some friction.

9. The feed was set to 81.3 μm/turn, (0.0032" / turn) for these three polarizers.

10. "Orange" Epoxy, #04007, by Hardman, Inc.

11. Two wrappings were made with this method and one of the polarizers was irrevocably destroyed during the application of the epoxy.

12. The theoretical value of k_2 was difficult to dermine because of the lack of resolution in the graphs of reference 6.

13. Polarizers were specifically designed for use in an experiment involving a millimeter wave measurement of the Rydberg constant.

14. D.H. Martin and J. Lesurf, Infrared Physics, 18, 1978, p. 405.

15. Yariv, Introduction to Optical Electronics, Holt, Rinehard and Winston, New York, 1976, p. 33.

16. Molectron, Model P1-42 CC.

17. Analysis was done using C-PLOT™. The algorithm may be found in Bevington, Data Reduction and Error Analysis for the Physical Sciences, McGraw-Hill, New York, 1969, p. 235.

18. Millitech®, Millimeter and Submillimeter Components, Instruments, Subsystems, 1986, pp. 86/9 - 30. Model PZE-XX-F, current price:$1950 per polarizer (with frame).

19. Published data from reference 2 and reference 3 were also examined, but the experimental parameters were too different to make any valid comparisons.

FACULTY SPONSOR

Dr. Daniel Kleppner
Lester Wolfe Professor of Physics
Department of Physics
Massachusetts Institute of Technology
Cambridge, MA 01239

AN ANALYSIS OF THE FACTORS AFFECTING RADON CONCENTRATION IN HOMES IN DECORAH, IOWA

Rahid Karim and Atul Wahi
Department of Physics
Luther College
Decorah, IA 52101

ABSTRACT

We conducted a survey of radon concentrations in homes in the Decorah, Iowa area. We correlated the concentrations with factors such as basement type, clay percentage in the soil, cracks in the basement walls and underlying geological formations. The results of the study suggests that only the cracks are a significant factor in determining the radon concentration in homes in Northeast Iowa. Preliminary analysis of the data suggests a significant statistical difference exists in radon levels in the east and west portions of the survey area.

INTRODUCTION

Radon was first discovered by Rutherford. It can be obtained by gently heating a sample of radium bromide. [1] Found in Group O of the periodic table with the inert gases, its physical properties resemble the other members of the group : He; Ne; etc. It is colorless, odorless and chemically inert. As is common with most elements with such large atomic weight, radon is radioactive.

There are 27 different isotopes of radon, ranging from Rn^{200} to Rn^{226}. Its three well known isotopes are Rn^{219}, Rn^{220} and Rn ^{222}. The most abundant isotope, Rn^{222}, is produced by the decay of the most prominent radium isotope Ra^{226}, which, in turn, is the product of the most abundant isotope of uranium, U^{238}. The decay scheme of Rn^{222} is shown in Figure 1.

Uranium is ubiquitous in the earth's crust, being present in virtually all forms of rock and soil. Therefore, its daughter, Rn^{222}, is also found abundantly in the soil as a gas trapped in the pore spaces of the rock and soil. However, its concentration in the ambient air is low.

The relatively long half life of Rn^{222} (3.8 days) enables it to diffuse out of the earth's crust. Its abundance in the atmosphere depends upon the depth at which it is formed, the concentration of uranium in the rock and soil and the permeability of the ground to radon. Approximately 10% of the radon formed in the top meter of soil escapes into the atmosphere. [2] Furthermore, soil gas,

Atul Wahi is a senior computer science and mathematics major with a minor in Physics. He plans on attending graduate school in the spring of 1991. Rahid Karim graduated in January, 1990 with a major in computer science and a minor in physics. He too plans on attending graduate school

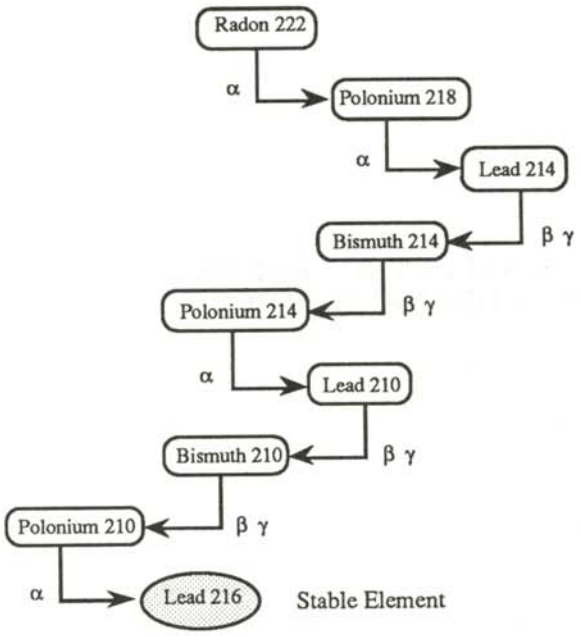

Figure 1
Decay scheme for Ra222 showing the radioactive daughter products and the types of radiation produced.

entering homes via cracks or plumbing penetrations, can lead to the build up of radon in the lower levels of a home.

While radon itself is rather inert, the decay products of radon attach themselves to other atoms readily. Rn^{222} atoms, and consequently the radioactive daughter products, that escape into the atmosphere and are inhaled, have been linked to lung cancer. The Environmental Protection Agency estimated in 1986 that from five thousand to twenty thousand lung cancer deaths a year in the United States may be attributed to radon. [3]

DESCRIPTION OF RESEARCH

The high concentrations of radon documented in other parts of the country inspired us to conduct a radon concentration survey in the Decorah, Iowa area. [4]
Decorah is located in northeast Iowa, about 70 miles south of Rochester, MN. It is located in a river valley with about 200 feet of local relief. The bedrock geology in this area is mostly limestone and shale.

The survey was conducted with canisters which contained activated carbon to which the radon daughters could become attached.[5] The contents of the charcoal after exposure was determined by a commercial enterprise.[6] These detectors are relatively inexpensive and have an accuracy of about 25%.

We conducted two separate surveys. The first survey, conducted in January 1988, was of twenty four homes of faculty and staff members of Luther College. These homes were uniformly spread out over Decorah. In this survey, we placed the detectors in the first floor living area of the house. After exposure for one week, they were sent for analysis of the radon value.

The second survey, completed in January, 1989 and discussed in detail in this paper, included sixty nine houses. We mailed the detectors and a questionnaire to be filled out by the home owner to homes evenly distributed over the Decorah area. The questionnaires were to be returned to us while the canisters were to be sent directly to the processing lab by the homeowner. The detectors were placed in the basement in accordance with EPA guidelines. [7] The questionnaire asked the home owner for information on

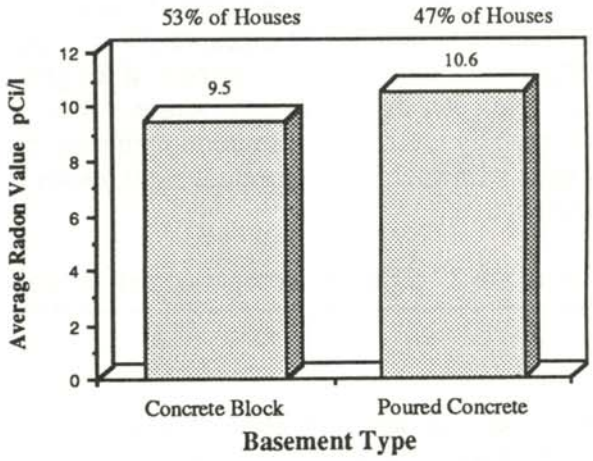

Figure 2
Dependence of the radon value on the type of basement construction. The numbers on the top of the histogram show the percentage of homes with each kind of basement construction

the basement construction, existence of cracks, unpaved crawl spaces and sump pumps; the favored entry routes for radon gas into homes. The data were entered into a spreadsheet for analysis.

RESULTS

The first survey produced an average radon value of 4.5 pCi/l, somewhat higher than the EPA 'action guideline' of 4.0 pCi/l established for detectors placed in the basement of a home.[8] The high radon values found provided the motivation for the second, more thorough, investigation.

The average reading for the second survey was a radon value of 9.9 pCi/l The higher average from the second survey reflects the tendency of radon to accumulate in the basement of homes because of its large atomic weight.

Figure 1 is a plot of radon values (activity per liter of air) vs the type of basement. The histogram shows that the radon values were, contrary to our original thoughts, independent of the type of construction of the basement. Since only a small number of homes reported sump pumps and unpaved crawl spaces, we could not draw conclusions based on these two parameters.

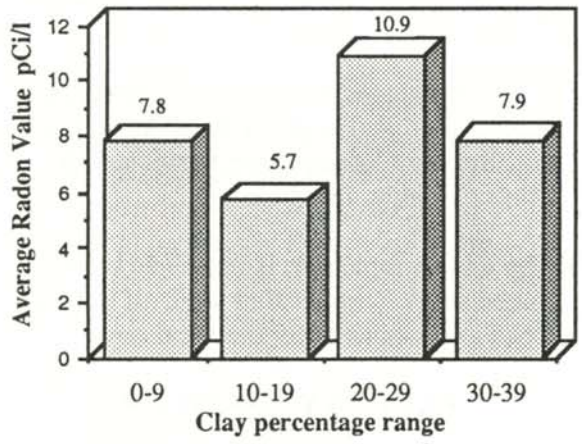

Figure 3
Dependence of randon value on the percentage of clay in the soil around the home.

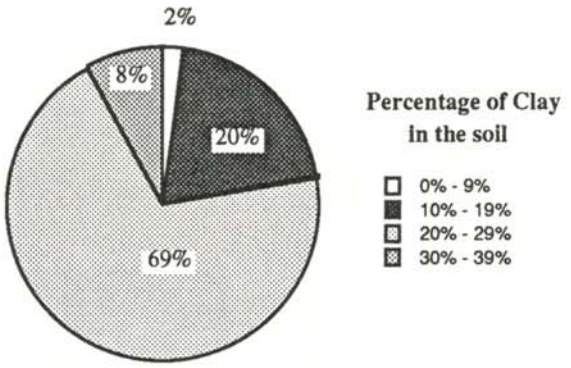

Figure 4
Percentage of homes tested as a function of the percentage of clay in the soil surrounding the home.

Figure 3 shows how the average radon values depend upon the percentage of clay in the soil surrounding the home. [9] The data do not show any correlation between the percentage of clay in the soil and the radon values. However, since only 2% of the homes were constructed on soils falling in the 0 - 9% clay content range (see Figure 4), caution is advised in drawing any firm conclusions about the dependence of radon levels on clay content from our data.

Figure 5 shows the dependence of the radon value on whether or not cracking was reported in the basement. The data indicate that the presence of cracks has a significant influence on the radon value. This supports the argument that cracks in the basement walls allow the radon gas to penetrate into the basement of a home. The overriding effect of the cracks in the walls on the radon values may obscure any difference due to other factors, such as basement construction and clay percentage in the soil.

We also investigated the possibility of a regional variation in radon concentration across the survey area. On a map, based on the city engineer's map of Decorah, we located each participating home and plotted its radon value. A visual scan of the radon values suggested a difference between radon concentrations in the east and west portions of Decorah.

We found the mean radon value of 19 homes in the west to be (4 ± 2) pCi/l and the mean of 25

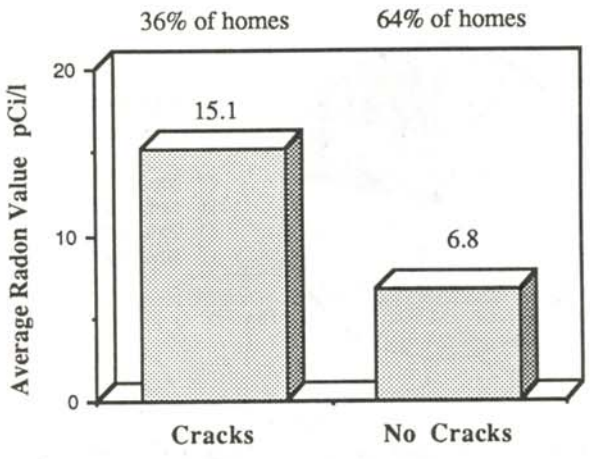

Figure 5
Radon value dependence upon whether or not the basement showed indication of cracking. The values at the top of the histogram show the percentage of homes in each catagory.

homes in the east at (11 ±9) pCi/l.[10] These data eliminated the crack factor as the basements with cracks were found to be uniformly distributed across the entire survey area.

We further analyzed the data by calculating the natural log of the radon values and computing the mean and standard deviation of these values. This has the effect of compressing the values over a narrow range which more closely approximates that of a normal distribution. These data were then compared statistically using the T test.

We found a probability of only 0.001 that the means for the two areas are the same, assuming that our population means are a reasonable approximation of the true mean. A significant statistical difference seems to exist between the two areas which is unrelated to parameters such as cracks in the basement walls. Some care should be taken with this conclusion as the T test assumes a large and truly random sample of the population. Neither of these conditions were completely satisfied by this data set.

ACKNOWLEDGEMENTS

The authors would like to thank Dr. Richard Kellogg for his guidance and time spent helping us. We also would like to thank John Laughlin (Luther College graduate, 1989) for his help in this research. Further, we are greatly indebted to Luther College for providing us with the funds for this research.

REFERENCES

1. Ernest J. Baldwin, Principles of Inorganic and Analytical Chemistry, D. Van Nostrand Co, Inc., New York, 1940 p. 112.

2. D. Bodansky, M. Robkin and D. Stadler, Indoor Radon and its Hazards, University of Washington Press, 1987, p. 3.

3. Environmental Protection Agency, A Citizen's Guide to Radon, What It Is and What To Do About It.

4. Personal Communication, Tom Peake, U.S. Environmental Protection Agency, Washington, DC, 1989.

5. The canisters were obtained from and measured by Best Inspect, 5410 William Flynn Highway, Rt. 8, Gibsonia, PA 15044.

6. *Ibid.*

7. *Op. Cit.*, Environmental Protection Agency, p. 61.

8. *Op. Cit.*, Environmental Protection Agency, p. 7.

9. Clay percentages were obtained from data supplied by the Department of Agriculture, Soil Survey Conservation Service, Winneshiek Country, Iowa.

10. The total sample size is not 69 as we eliminated several homes that were all on one road and would skew the areal coverage.

FACULTY SPONSOR

Dr. Richard Kellogg
Department of Physics
Luther College
Decorah, IA 52101

COMPETITION BETWEEN DE-EXCITATION PATHWAYS AFTER 7P AND 7D EXCITATION OF CESIUM

John M. Stewart
Department of Physics
Davidson College
Davidson, NC 28036

ABSTRACT

Competition between different de-excitation paths was observed after excitation to the 7P and 7D states in Cs. This competition resulted either from interference between different types of emission or from reduced gain due to a decrease in the population inversion between upper and lower states.

TYPES OF EMISSION

AMPLIFIED STIMULATED EMISSION

Amplified Stimulated Emission can occur when an excited atom spontaneously emits a photon in a region where many other atoms are in identical excited energy state as the original atom that emitted the photon. The photon then causes other atoms to emit photons which have the same phase and energy as the initial photon. This type of emission propagates parallel (forward) and antiparallel (reverse) to the direction of the exciting laser beam. A schematic energy diagram of this process is shown in Figure 1A.

John Stweart graduated from Davidson College with Honors in Physics in 1989. This work composed part of his Honor's Thesis. He is currently on scholarship in the Ph.D. program in Electrical Engineering at the Georgia Institute of Technology

RAMAN

A Raman process involves a single photon excitation of a virtual state. A hyper-Raman process involves a double photon excitation of a virtual state [1]. The virtual state has an extremely short lifetime. The lifetime is given roughly by the Heisenberg uncertainty principle:

$$t = h/\Delta E, \qquad (1)$$

where h is Planck's constant and ΔE is the energy difference between the atomic resonance and the energy of the incident photon. [2] The atom emits a photon quickly unless the exciting photon's energy is very close to the atomic resonance.

The energy of the Raman photon changes at a one to one ratio with the energy of the exciting laser photon, while the hyper-Raman photon's energy changes with a ratio of two to one. Raman and hyper-Raman emission also propagate in the forward and reverse directions with re-

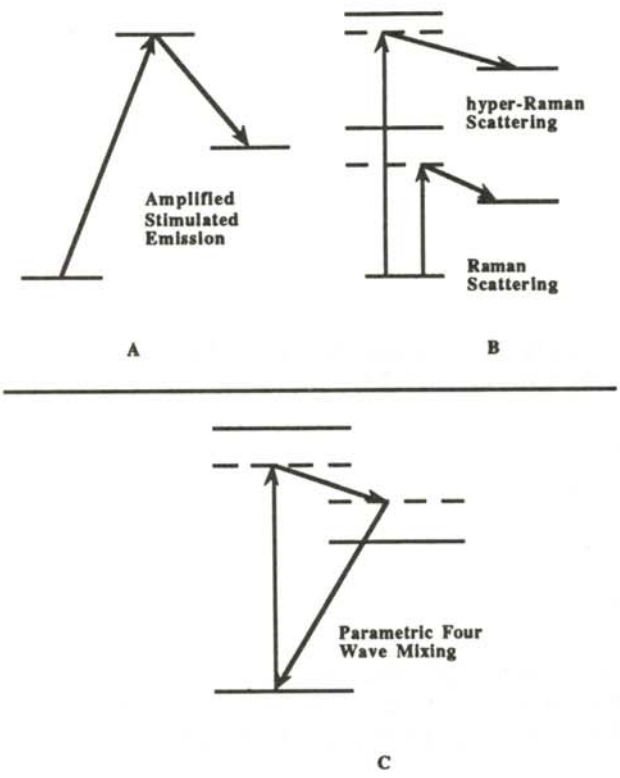

Figure 1
Energy diagrams showning the conditions for the various types of emission mechanisms

spect to the incident laser beam. A schematic energy diagram of these processes is shown in Figure 1B.

PARAMETRIC FOUR WAVE MIXING

In parametric four wave mixing (PWFM), two externally supplied photons, the sum of whose energy is the same as that of a virtual state, excite that state. The atom then produces a third photon by dropping to a second virtual state, and eventually produces a fourth photon when falling back to its initial energy state [3]. A schematic energy diagram of this process is shown in Figure 1c.

Two conditions must be met for this parametric process to occur. First, energy must be conserved, so the sum of the emitted photon energies must equal the sum of the laser photon energies. Second, the sum of the propagation vectors of the four photons must be zero to meet phase matching conditions with the incident laser photons. The propagation vector points in the direction that a photon travels and has a magnitude of ν/c, where ν is the frequency of the photon and c is the phase velocity of the photon.

Consider the situation where a number of photons of different energies are incident on a gas of cesium atoms. Some of the photons will have energies that match energies of allowed transitions in cesium. These photons will have a high probability of interacting with the cesium atoms, so they see an index of refraction different from 1. Other photons, whose energy do not match any transitions in cesium, will pass through the cesium gas almost unaffected. These photons will see an index of refraction close to 1. This dependence of the index of refraction on the energy (and hence the frequency) of the photons is called dispersion. This effect can cause a nonzero sum of propagation vectors in PFWM.

There are two ways that PFWM photons can compensate for dispersion effects. First, the photons can adjust their angles of propagation, changing the sum of the propagation vectors. This sort of emission propagates outward in the shape of a cone. Second, the PFWM photons can propagate axially, but the photons change their energies to find points on the dispersion curve where phase matching is possible [4]. In both cases, the emission does not propagate in the reverse direction because the phase matching condition is not satisfied.

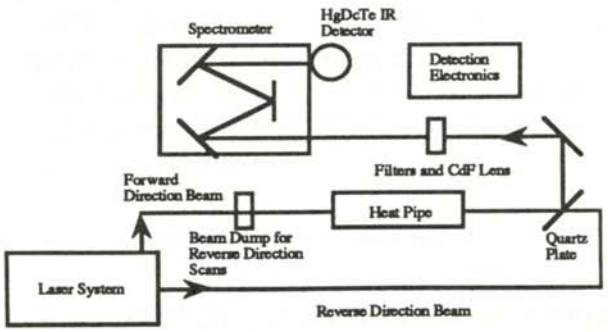

Figure 2
Schematic diagram of the apparatus used, showing both forward and reverse direction scans.

THE EXPERIMENT

A Nd:YAG pumped dye laser system, shown in Figure 2, was used to generate laser light near the single photon 7P resonance and the two photon 7D resonance in Cs. The laser light was directed through a heat pipe oven, operating at 600K, with a Cs vapor pressure of 4 Torr. A quartz plate, placed at a 45° angle to the beam, directed some (about 4%) of the laser emission and some of the emission from the gas in the heat pipe to a spectrometer. This beam first passed through a series of filters, chosen to pass a selected band of wavelengths. A CaF lens then focused the emission beam into an ISA spectrometer, equipped with either a 300 lines/mm or 120 lines/mm grating, depending upon the which wavelength band was to be analyzed.

A HgCdTe infrared detector, in conjunction with a boxcar integrator, was used to examine the output from the spectrometer. An IBM AT computer moved the spectrometer grating and recorded the IR signal at each increment. The computer also controlled the laser frequency, so scans could be made over a series of emission wavelengths and at various laser detunings. When we wished to detect reverse emission, the laser beam was directed through the back side of the quartz plate and then into the heat pipe. In this situation, the emission photons traveling in the opposite direction to the incident laser photons were reflected into the filter and spectrometer system.

The system was calibrated using emission from the 8S -> 6P and 7S -> 6P transitions. These states were least affected by the strong fields produced by the laser.

OBSERVATIONS

7P EXCITATION

An interference effect was noted after single photon excitation at energies near either of the 7P fine structure states. In this case, the 7P->7S->6P and the 7P->5D->6P (see Figure 3) routes competed with each other. When the laser was tuned to either 7P fine structure lines, the 7P->7S and 7S->6P emissions were weak,

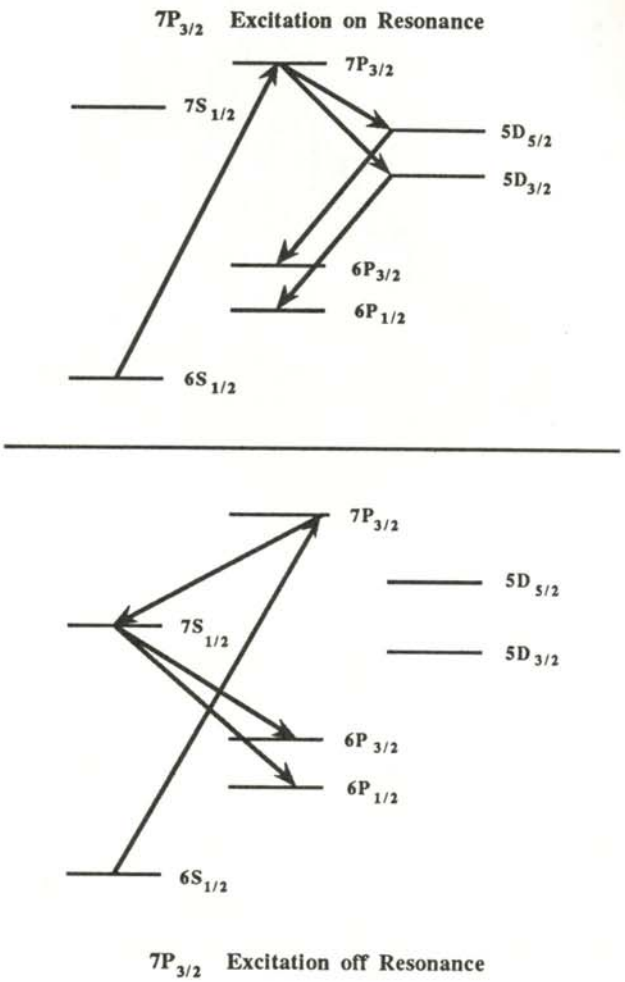

Figure 3
Schematic Energy diagram showing the various competing de-exciting modes after a $7P_{3/2}$ excitation

while the 7P->5D emission peaked. The opposite occurred off the resonance; the 7P->5D emissions were weak and the 7P->7S and 7S->6P emissions grew strong.

Figure 4 shows a three dimensional plot of the intensity of the $7P_{3/2}$->$7S_{1/2}$ emission as a function of the wavelength of the emission and the wavelength of the incoming laser photon beam. For this case, $\Delta E_{Emission}/\Delta E_{Laser} = 1$. This emission was also visible in the reverse direction, so it was attributed to Raman scattering. The dip in the intensity of the Raman emission was the first indication of interference between the two pathways.

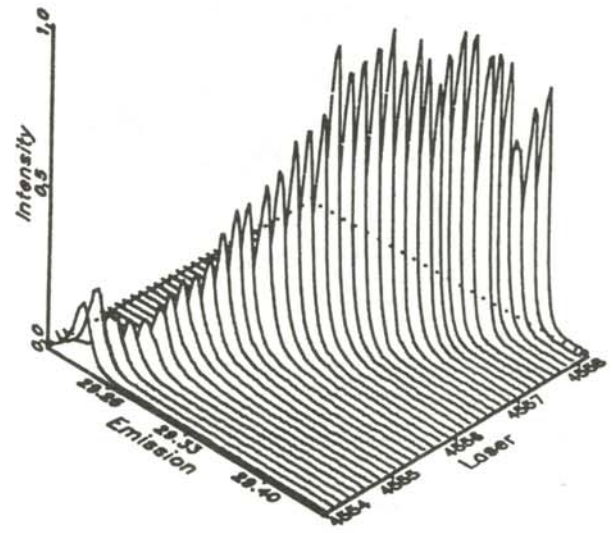

Figure 4
A plot of intensity of emission vs wavelength of the emitted photon vs wavelength of the incident photon for the $7P_{3/2}$->$7S_{1/2}$ transition. Notice the dip in the resonance.

The competition between the two pathways is dramatically illustrated in Figure 5. The $7S_{1/2}$->$7P_{1/2}$ emission dips where the $7P_{3/2}$->$5D_{3/2}$ emission sharply peaks. A third emission scan at 6.34 μm revealed a $7P_{3/2}$->$5D_{3/2}$ emission which also peaked sharply on resonance.

All of the emission lines shown in Figure 6 were visible in both the forward and reverse directions. Both the $7S_{1/2}$->$6P_{1/2}$ and the $7P_{3/2}$->$5D_{5/2}$ emissions had a non-tuning component visible over large laser detunings. These components were probably due to ASE. In addition to the ASE, the $7P_{3/2}$->$5D_{3/2}$ emission had a small side peak with a $\Delta E_{Emission}/\Delta E_{Laser} = 1$, indicating a Raman process was taking place.

The dip in Figure 5 can be explained in the following way. On resonance, the 5D->6P emissions may have filled both 6D fine structure states, lowering the population inversions for the 7S->$6P_{1/2}$ and 7S->$6P_{3/2}$ transitions. With the emissions blocked, the 7S population would have grown, suppressing the Raman emission into the 7S state and creating the dip.

7D EXCITATION

When the laser was tuned alternately to the two photon $7D_{5/2}$ and $7D_{3/2}$ resonances, a flip-flop was observed in the fine structure of the $8S_{1/2}$->7P and 7D->7P emissions: $7D_{5/2}$ excitation generated only $8S_{1/2}$->$7P_{1/2}$ and $7D_{5/2}$->$7P_{3/2}$ emissions, while $7D_{3/2}$ excitation resulted in $8S_{1/2}$->$7P_{3/2}$ and $7D_{3/2}$->$7P_{1/2}$ emissions.

This phenomenon was unusual because after $7D_{5/2}$ excitation, the total angular momentum J did not change in the $8S_{1/2}$->$7P_{1/2}$ transition. Under normal conditions, the total angular momentum is most likely to change by 1, leaving the atom in the $7P_{3/2}$ state. However, this transition was not observed, so interference from another de-excitation pathway must have been present.

A possible explanation, similar to the interpretation of the 7P competition for the suppression of the $8S_{1/2}$->7P3/2 transition, is that the $7D_{5/2}$->$7P_{3/2}$ emission reduced the

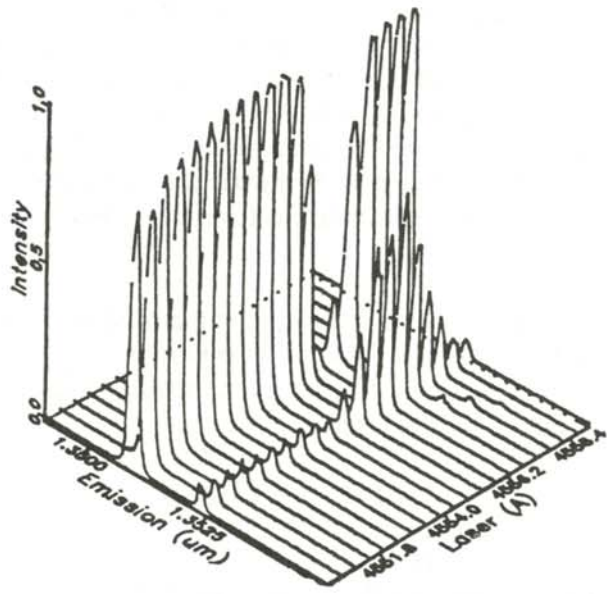

Figure 5
A plot of intensity of emitted radiation vs emission energy vs incident photon energy. Notice the dip in the $7S_{1/2}$->$6P_{1/2}$ emission as the $7P_{3/2}$->$5D_{5/2}$ emission peaks.

$8S_{1/2}$->$7P_{3/2}$ population inversion to the point where ASE ws no longer possible. Since selection rules prohibit the $7D_{5/2}$ -> $7P_{1/2}$ transition, the $8S_{1/2}$ ->$7P_{1/2}$ transition remained open as a viable de-excitation path. Emission from this transition was observed.

A similar blocking occurred after the $7D_{3/2}$ excitation, although in this case, both branches could change their total angular momentum by 1 and still end up in different fine structure states. Neither the $7D_{3/2}$->$7P_{3/2}$ nor the $8S_{1/2}$->$8P_{1/2}$ transitions were observed following the $7D_{3/2}$ excitation. While low transition probabilities may explain the absence of these emissions, competition between the two paths could have added a suppression mechanism.

Although population buildup seems to explain the observed emission fairly well, interference between PFWM and ASE is also a possibility. Unlike the emission associated with 7P excitation, PFWM near the $7D_{5/2}$->$7P_{3/2}$ resonance was present in emission scans. An ASE component was visible in both the forward and reverse directions over a wide range of laser detunings. A strong PFWM component, tuned irregularly in the forward direction only, also appeared.

A $7P_{3/2}$->$6S_{1/2}$ blue emission with irregular tuning characteristics complemented the IR PFWM emission. This emission was only visible in the forward direction and had a conical shape, indicating phase matching by angle adjustment. No resonant ASE was observed, since resonant $7P_{3/2}$->$6S_{1/2}$ emission would have been trapped by the high Cs density in the heat pipe.

SUMMARY

A variety of studies on competition due to quantum interference have been conducted. [5,6] In particular, a study by Wunderlich, et.al. [7] has shown that ASE and hyper-Raman scattering can be suppressed by PFWM fields within the atom. In this case, the wave function for PFWM cancels the wave functions for ASE and hyper-Raman scattering.

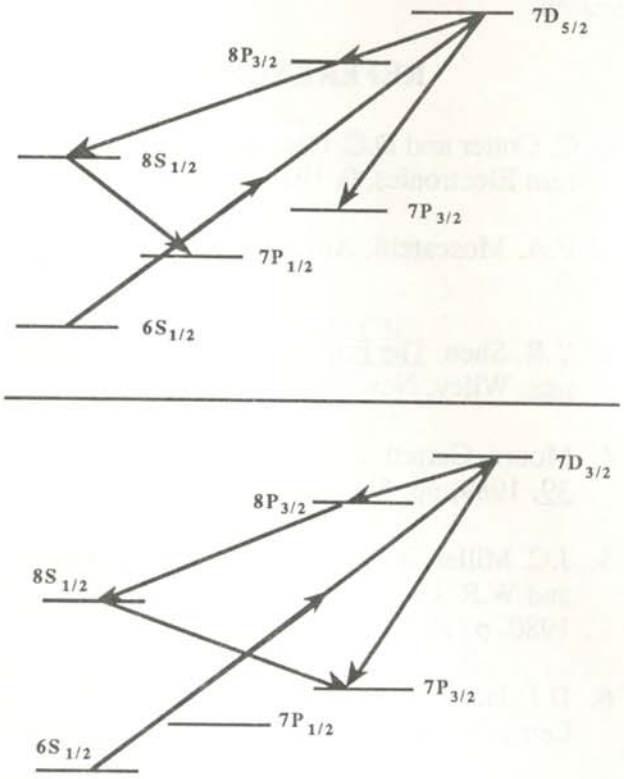

Figure 6
Competing modes of de-excitation after a 7D excitation, showing emission on and off resonance.

Additional experiments are planned to determine the mechanism causing this suppression. The laser beams could be counter propagated through the heat pipe. Counter propagating laser beams destroy the phase matching conditions necessary for PFWM. If the competition persisted after PFWM ceased, population build up would be confirmed as the suppressing mechanism. A second experiment would utilize a low power diode laser probe, tuned at the $8S_{1/2}$->7P resonance. If the 7P states become populated, the Cs will absorb the diode laser beam and no probe light would emerge from the opposite end of the heat pipe.

ACKNOWLEDGEMENTS

The author wishes to thank Dr. Wolfgang Christian for his support during this study. He also acknowledges the support of the Howard Hughes Medical Foundation for funding this re-

search.

REFERENCES

1. C. Cotter and D.C. Hanna, Opt. and Quantum Electronics, 9, 1977, p. 509-518

2. F.A. Moscatelli, Am. J. Phys., 54, 1986 p. 1.

3. Y.R. Shen, The Principles of Nonlinear Optics, Wiley, New York, 1984, p. 117.

4. Moore, Garrett and Payne, Phys. Rev. A, 39, 1989, pp. 3692-3695.

5. J.C. Miller, R.N. Compton, M.G. Payne and W.R. Garrett, Phys. Rev. Lett., 45, 1980, p. 114.

6. D.J. Jackson and J.J. Wynne, Phys. Rev. Lett., 49, 1982, p. 543.

7. Wunderlich, Moore, Garrett and Payne, to be published.

FACULTY SPONSOR

Dr. Wolfgang Christian
Department of Physics
Davidson College
Davidson, NC 28036

Post Use Book Review

THERMODYNAMICS, AN ENGINEERING APPROACH

Yunus A. Cengel and Michael A. Boles
McGraw-Hill, Inc., 1989

Reviewed by:

Tracey L. Coble
Thiel College
Greenville, PA 16125

When browsing through this text, one notices that it contains many figures and diagrams, it is not full of equations. Instead of using bold print, red ink is used for headings and important words. The book appears interesting to read, not dry like many mathematics manuals.

One problem with many physics texts is that they base their discussion on how variables act, meticulously building equations, but leaving out discussion of the physical world. The result is a text that is hard to follow and often quite boring to read. **Thermodynamics, An Engineering Approach** is different. Discussion is based on physical processes into which variables are introduced when necessary. The book does not presume a lot of previous knowledge of specific concepts. Most of the constants, units and theories are given a short explanation before being used.

A beginning physicist or engineer must learn to follow complex material, but must also be able to understand the text. **Thermodynamics, An Engineering Approach** balances these two needs quite well. When necessary, the authors include derivations, but there is always enough English inserted to make them fairly easy to follow. Complicated mathematics are not allowed to bog down discussions.

As the title suggests, the book concentrates on applications. Discussion of physical laws usually includes physical examples that bring theory and the real world together, making the theory easier to understand and remember. To add to this process, "Blondie" cartoons are scattered lavishly throughout the text. These cartoons serve as a refresher for those who tend to nod off while reading.

The problems at the end of each chapter include many concept questions. They are distributed among the problems so as to follow the progress of the chapter, just as the problems do. These concept questions are marked with a 'C' and are numbered in red so that they are easy to pick out. For the most part, they deal with general system reactions, so more than a facility with equations is required to answer them. These special questions demand significant thought, even on the part of the professor, and can be used to begin class discussions.

Every text used in the United States must deal with the problem of the English system of units. While most physicists could easily ignore them, engineers have to learn how to use them. This

text acknowledges this problem in the preface. For the most part, the solution is similar to that used in other books: discussion in metric, but the English units in parentheses, and do only a very few problems in the English units. However, this text adds at the end of each chapter many English unit problems. Each one, marked with an 'E' as a warning signal, is identical to the preceeding metric problem, except for the numbers and the units. In this way, each problem in the book is available for use by those who shun the English system. Students who have trouble with the English unit system can try the problem in the metric system first. There are two sets of tables of properties in the back of the book , one in each of the two separate unit systems. The tables of properties themselves are quite extensive. They are calibrated with each other so that it is possible to use two or more tables for any problem.

Inside the back cover of the text is an 'IBM compatible' software package, containing programs that calculate for many substances values for intensive and extensive properties when the user provides two of them. This package, however, is little more than a curiosity. Since the temperature - pressure range is quite limited, it is of little use in solving most problems. The tables are much more extensive and more readily handy than an IBM compatible computer.

The overall effectiveness of **Thermodynamics, An Engineering Approach** is very good. The text is readable and contains examples that help the student relate to the material. The concept questions and problems appear well chosen to test and improve the student's knowledge of thermodynamics. Combined with in-class discussion, it provides for an excellent thermodynamics course.

The Journal of Undergraduate Research in Physics

The *Journal of Undergraduate Research in Physics* is the journal of Sigma Pi Sigma and the Society of Physics Students. It is published by the Physics Department of Guilford College, Greensboro NC. Inquiries about the journal should be sent to the editorial office.